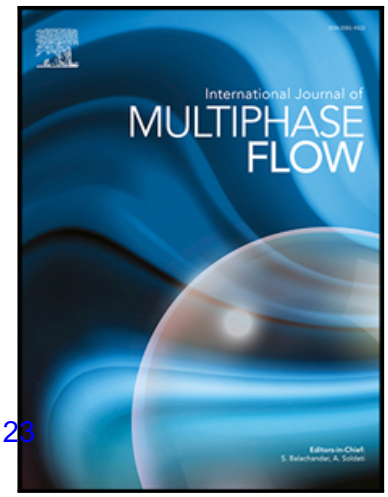

Numerical investigation of the aerodynamic breakup of a parallel moving droplet cluster

Dionisis Stefanitsis , George Strotos , Nikolaos Nikolopoulos , Manolis Gavaises

PII: S0301-9322(19)30246-0
DOI: https://doi.org/10.1016/j.ijmultiphaseflow.2019.103123
Reference: IJMF 103123

To appear in: *International Journal of Multiphase Flow*

Received date: 15 April 2019
Revised date: 23 July 2019
Accepted date: 24 September 2019

Please cite this article as: Dionisis Stefanitsis , George Strotos , Nikolaos Nikolopoulos , Manolis Gavaises , Numerical investigation of the aerodynamic breakup of a parallel moving droplet cluster, *International Journal of Multiphase Flow* (2019), doi: https://doi.org/10.1016/j.ijmultiphaseflow.2019.103123

Highlights

- Two- and three-dimensional simulations of the aerodynamic breakup of a parallel moving droplet cluster at representative engine conditions.
- Droplet proximity becomes important for non-dimensional distances between the droplets equal to or lower than 5.
- The breakup initiation time of a droplet in a cluster is lower than that of an isolated droplet, while the drag coefficient is higher.
- For very low distances between the droplets (H/D_0<1.5), the critical We number (minimum We number leading to breakup) of a droplet in a cluster becomes lower than that of an isolated droplet at the same conditions.

Numerical investigation of the aerodynamic breakup of a parallel moving droplet cluster

Affiliations

Dionisis Stefanitsis[*1,2,], George Strotos[3], Nikolaos Nikolopoulos[1], Manolis Gavaises[2]

[1]Centre for Research and Technology Hellas/Chemical Process and Energy Resources Institute (CERTH/CPERI), Egialeias 52, Marousi, Greece

[2]City University London, School of Engineering and Mathematical Sciences, Northampton Square, EC1V 0HB London, UK

[3]Technological Educational Institute of Thessaly, Mechanical Engineering Department, 41110 Larissa, Greece

[*]Corresponding author: stefanitsis@certh.gr

gstrot@teilar.gr, n.nikolopoulos@certh.gr, M.Gavaises@city.ac.uk

Abstract

The present work examines numerically the aerodynamic breakup of a cluster of Diesel droplets moving in parallel with respect to the gas flow. Two- and three-dimensional simulations of the incompressible Navier-Stokes equations together with the VOF method are performed for Weber (*We*) numbers in the range of 5 up to 60 and non-dimensional distance between the droplets (H/D_0) ranging from 1.25 to 20. The numerical results indicate that the proximity of droplets affects their breakup for distances $H/D_0 \leq 5$. For low droplet proximity distances ($H/D_0 \leq 2.5$), the droplets experience the so-called shuttlecock breakup mode, which has been also identified for droplets in tandem formations in a previous authors' work and is characterized by an oblique peripheral stretching of the droplet. With decreasing H/D_0 the breakup initiation time decreases, while the drag coefficient increases relative to that of isolated droplets. When the distance between the droplets is low enough ($H/D_0 < 1.5$), this can result in critical *We* number, i.e. minimum *We* number leading to breakup, lower than that of an isolated droplet at the same conditions.

Keywords

Cluster droplet breakup; Diesel; drag coefficient; breakup time; critical *We*.

Nomenclature

Roman symbols

B	Average dimensionless deformation rate [-]
C_d	Drag coefficient [-]
D	Droplet diameter [m]
D_{cr}	Cross-stream droplet deformation [m]
D_{str}	Streamwise droplet deformation [m]
H	Cross-stream distance between droplet centres [m]
L	Streamwise distance between droplet centres [m]
N	Viscosity ratio [-]
U	Velocity [m/s]
V_{cell}	Volume of cell [m^3]
We	Weber number [-]

Greek symbols

α	Liquid volume fraction [-]
ε	Density ratio [-]
μ	Dynamic viscosity [kg/(m·s)]
ρ	Density [kg/m^3]
σ	Surface tension [N/m]

n_{cells}	Number of computational cells [-]
Oh	Ohnesorge number [-]
P	Pressure [Pa]
Re	Reynolds number [-]
S	Droplet surface area [m^2]
T	Temperature [K]
t	Time [s]
t^*	Non-dimensional time [-]
t_{br}	Breakup initiation time [s]
t_{sh}	Shear breakup timescale [s]

Subscripts

0	Initial
cl	Cluster
cr	Critical
d	Droplet
g	Gas phase
is	Isolated droplet
L	Liquid phase
max	Maximum
rel	Relative

1 Introduction

Droplet deformation and eventually breakup is encountered in various systems and applications [1]. The non-dimensional numbers usually utilised for classifying the breakup outcome of isolated droplets are the Weber (*We*), Ohnesorge (*Oh*) and Reynolds (*Re*) numbers as well as the density (ε) and viscosity ratios (*N*) of the two phases [2]; these are defined as:

$$We = \frac{\rho_g U_{rel,0}^2 D_0}{\sigma} \qquad Oh = \frac{\mu_L}{\sqrt{\rho_L \sigma D_0}} \qquad Re = \frac{\rho_g U_{rel,0} D_0}{\mu_g} \qquad \varepsilon = \frac{\rho_L}{\rho_g} \qquad N = \frac{\mu_L}{\mu_g} \tag{1}$$

The breakup timescale can be also approximated by the non-dimensional correlation proposed by Nicholls and Ranger [3]:

$$t_{sh} = \frac{D_0}{U_{rel,0}} \sqrt{\varepsilon} \tag{2}$$

The aerodynamic breakup of isolated droplets has been thoroughly investigated (see for example [2] among many others); more recently the breakup of droplets in tandem formations has been also reported [4-6]. On the other hand, not much focus has been paid to the breakup of droplets moving in parallel with respect to the surrounding air; such collective droplet cluster motions can be considered more representative for the conditions typically realised in fuel sprays consisting of a large number of droplets [1]. In these formations apart from the non-dimensional streamwise distance between the droplets (L/D_0), also the cross-stream one (H/D_0) can be speculate to play a role; the *L* and *H* here correspond to distances between the droplet centres.

Regarding the hydrodynamic interaction between rigid particles, the experimental works of [7, 8] examined two particles exposed in parallel to a uniform flow of water, with non-dimensional distances between them (H/D_0) ranging from 1 up to 2.5 and *Re* number equal to 5,000. They studied mainly the flow around the particles and concluded that for H/D_0=1 (particles are in contact) the particles act as a rigid bluff body, while for $H/D_0 \geq 2$ the interaction between the shedding vortices is minimized as well as the effect of the jet-like flow occurring through them. Numerical studies of similar particle arrangements were performed by Folkersma et al. [9], Tsuji et al. [10], Ardekani et al. [11], Prahl et al. [12], Yoon and Yang [13] and by Jadoon [14]. The *Re* numbers examined range from $5 \cdot 10^{-7}$ up to 600, while the non-dimensional distance between the particles are in the range of 1 up

to 23. These studies focus mainly on the estimation of the force coefficients (drag, lift and pressure); it is generally concluded that the drag coefficient is higher for the parallel particle motion configuration compared to that of an isolated particle.

Turning now to studies referring to the parallel motion of droplets as opposed to solid particles, Temkin and Ecker [5] performed experiments with streams of water droplets at *Re* numbers in the range of 130 up to 600 and H/D_0 ranging from 3 up to 6 and streamwise distance between them L/D_0 from 1.5 up to 11. They observed that the wake of a droplet affects the drag coefficient of the trailing droplets that lie within a parabolic shape of $15D_0$ length and $1D_0$ width. Connon and Dunn-Rankin [15] studied experimentally the behavior of an isolated water droplet displaced radially from a droplet stream, and concluded that the droplet stream influences its surroundings for $H/D_0 \leq 15$ and $L/D_0 \leq 15$. Later, Zhao et al. [16] investigated experimentally the aerodynamic breakup of two water droplets arranged at various configurations with streamwise and cross-stream non-dimensional distances less than 3, while the *Re* number was equal to 2680 and the *We* equal to 12.3. They identified four breakup modes: i) coalescence, ii) puncture, iii) side-by-side and iv) no direct contact, and concluded that the fastest mode is the side-by-side, in which the droplets deform into a disk-like shape with their edges touching before the breakup occurs. This breakup mode is encountered for $H/D_0 \leq 2$.

Numerical simulations with droplets and solid spheres were performed by Kim and coworkers in [17, 18] for *Re*=100 and H/D_0 ranging from 1.5 up to 25. They found that for $H/D_0<9$ the drag coefficient of the droplets is higher than that of an isolated droplet at the same conditions. Prahl et al. [19] investigated numerically with the Volume of Fluid (VOF) method the interaction of two droplets exposed in a uniform flow of *Re*=100 and *We*=0.1 and 1. The streamwise distance between the droplets ranged from 1.5 up to 6, while the cross-stream one was equal to 1.5. It was found that for the parallel arrangement, the droplets experience higher drag force compared to the isolated droplet and also a weak attraction. Recently, Kekesi et al. [6] studied numerically using the VOF method the breakup of two liquid droplets arranged at various positions from tandem up to parallel, with *We*=20, *Re*=20 and 50, and L/D_0 and H/D_0 ranging from 1.5 up to 5. Three scenarios were identified for the breakup of the droplets: i) they collide and merge, ii) the secondary drop shoot through the primary drop and iii) the two drops behave independently. Finally, they found that for certain parallel configurations the breakup time is shorter than that of an isolated droplet. This was attributed to the increased velocity in the gap between the droplets, which results in enhanced shear at the droplet periphery.

The aforementioned numerical studies examined the breakup of two droplets moving in parallel to the air flow, while the current work investigates, for the first time, the breakup of a droplet inside a cluster of droplets; this can be considered as a typical droplet appearing at the inner part of a spray. More specifically, four droplets are simulated, or equivalently one droplet with symmetry boundary conditions (the equivalence of these configurations is proved in section 2.1), which represent an infinite cluster with the use of symmetry boundary conditions, as shown in Figure 2. Qualitative results are presented for the temporal evolution of droplet shape as well the breakup mode. In addition, a parametric study is performed with 2-D axisymmetric simulations for *We* and H/D_0 numbers as shown in Figure 1, where the previous numerical studies are presented as well. As it can be seen, a big portion of the map has not been investigated so far. The 2-D axisymmetric simulations are performed with a single droplet, while the effect of other droplets in their proximity is simulated

using symmetry boundary conditions. Results are presented for the effect of H/D_0 on the breakup mode, maximum surface area, critical *We* number (minimum *We* number leading to breakup), breakup initiation time and drag coefficient.

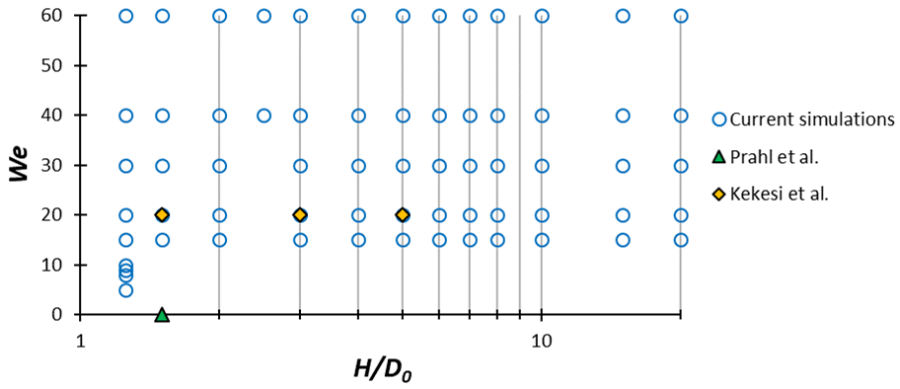

Figure 1. Examined *We* and H/D_0 numbers of the current and previous numerical studies.

The paper is structured as follows: initially, the computational setup and examined conditions are presented, followed by a section presenting the qualitative results as well as the results of the parametric study. Finally, the main conclusions are summarized in the last section of the paper.

2 Computational setup and examined conditions

The numerical model for the parallel droplet cluster motion and breakup solves the Navier-Stokes equations coupled with the Volume of Fluid (VOF) methodology [20] for tracking the interface between the liquid droplets and the surrounding gas. In order to model surface tension, the Continuum Surface Stress (CSS) model of [21] is utilized. Two-dimensional (2-D) axisymmetric and three-dimensional (3-D) simulations are performed with the commercial CFD tool ANSYS FLUENT v16 [22] along with the use of various User Defined Functions (UDFs); these account for the following: i) adaptive local grid refinement technique around the liquid-gas interface [23], ii) adaptive time-step scheme for the implicit VOF solver based on the velocity at the droplet interface [24], and iii) moving mesh technique based on the average velocity of the droplets. The CFD model has been developed and validated in previous works of the authors for a number of applications; among them are the free fall of a droplet [23], the droplet impingement on a flat wall [25] or a spherical particle [26-28], the aerodynamic droplet breakup [4, 24, 29-35] and the droplet evaporation [24, 31, 36]. It should be noted that he extension of the model validation for the case of droplet clusters is not possible since, to the author's best of knowledge, there are no experimental studies in the literature with droplet clusters, only a few featuring two droplets [5, 15, 16]. However, even with two droplets a 3D simulation would require approximately twice more computational resources than the simulation of four droplet quarters (3D-4 domain of Figure 2), in terms of CPU·hours. For this reason, and since the physical process is the same between the breakup of one and more droplets, we have assumed that the model is considered validated using only the case of the isolated droplet.

Figure 2 presents an infinite cluster of droplets arranged parallel to the air flow along with the computational domains utilized in the current work for its simulation: i) a 3-D domain with four droplet quarters (abbreviated as 3D-4), ii) a 3-D domain of a single droplet quarter (abbreviated as 3D-1), and iii) a 2-D axisymmetric domain. In all cases symmetry boundary conditions are utilized to

reflect the presence of surrounding droplets. In the following section (2.1) it is shown that the two examined 3-D configurations are equivalent, since they give identical results for a simulation at the same conditions. On the other hand, for the case of the 2D axisymmetric simulations, the adoption of a symmetry boundary condition does not strictly reflect the effect of the neighbour droplets at a 45^o direction (diagonal). However, the results using the 2-D domain are close to those of the 3-D simulations, even for very low values of H/D_0 (=2) (see section 2.1). For this reason, the 2D approach is utilized in the parametric study since it is much more computationally efficient than the other two, therefore making it possible to simulate the 67 examined cases within a reasonable time.

The droplet is initially stagnant, while air flows from the right boundary forcing it to move and deform. In Figure 2c and d, the distance measured from the centre of the droplet to the symmetry boundary conditions is equal to half the distance between the droplets ($H/2D_0$). In the depicted cases of Figure 2 this is equal to 1, and therefore H/D_0=2, while for a different H/D_0 the height of the domain should be adjusted accordingly, resulting in a new computational domain. The computational cells have a rectangular/hexahedron shape with a base grid resolution equal to 3 cells per radius (cpR), while 6 levels of local grid refinement (or 5 for the 3-D cases) are applied to obtain the desired resolution of 192cpR (or 96cpR for the 3-D) around the liquid-gas interface. The resolution of 96cpR has been found to be adequate for the simulations of droplet breakup as the average drop velocity, deformation and breakup initiation time change less than 1% when a finer grid is used. To give an idea about the grid size, the 3D-4 computational domain utilizes initially approximately 2.5 million cells, which increase up to 8.7 million at the end of the simulation, due to the use of the adaptive local grid refinement.

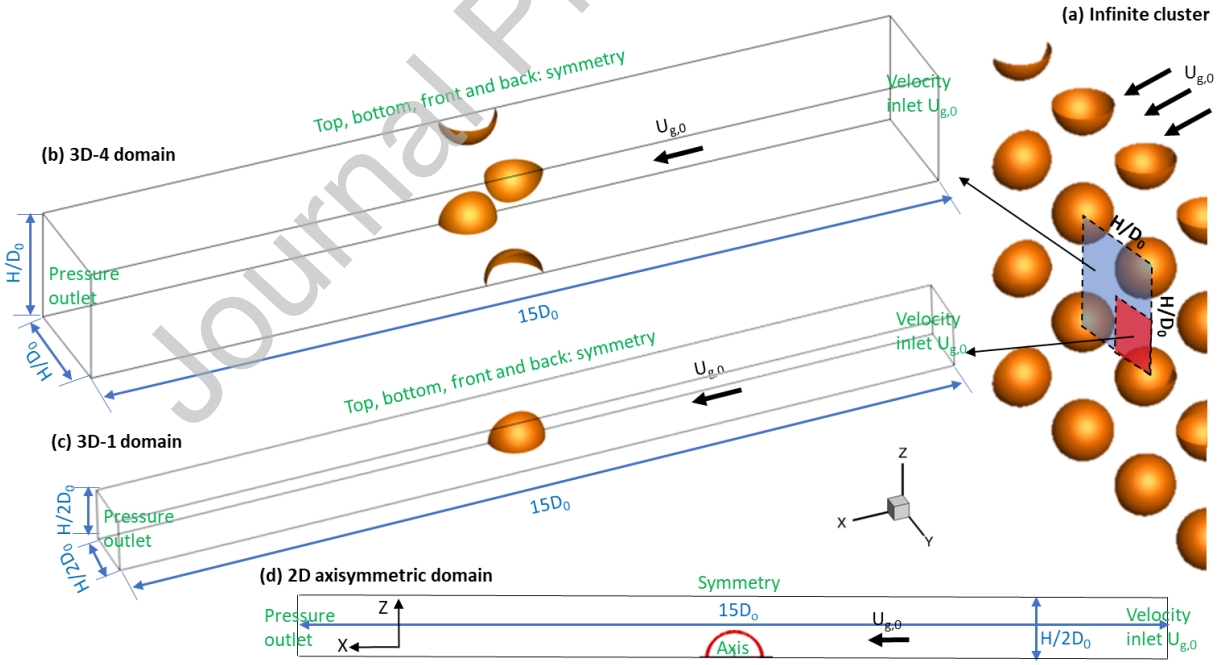

Figure 2. a) Actual configuration with an infinite cluster of droplets along with the computational domains and boundary conditions used in the simulations: b) 3D-4 domain, c) 3D-1 domain, and d) 2-D axisymmetric domain.

The simulations have been performed with Diesel fuel as liquid with properties taken from [37], using a four component surrogate and the PC-SAFT equation of state; a pressure of 40bar and a

temperature of 900K were considered for the estimation of gas properties, while a temperature of 335K was assumed for the liquid properties. These conditions correspond to those encountered in Diesel engines as presented in Table 1, along with the corresponding references used for their estimation. It should be noted that at such high air temperature, heating and evaporation of the droplets takes also place, but these were neglected in the current work, since its primary scope lies on the investigation of the effect of droplet proximity (similar to our previous work [38]). In view of that, any variations of droplet physical properties with temperature, including that of surface tension, were neglected, as the flow was considered to be isothermal. The justification for this approximation is given using the model of Strotos et al [31] to predict the heating and evaporation of a Diesel droplet in cluster formation with We=40 and H/D_0=2. The liquid physical properties used are those of Table 1, while the temporal evolution of droplet surface area is calculated based on the CFD simulations instead of the derived equation in [31]. For a typical duration of t=1.5t_{sh}, during which the droplet undergoes breakup as shown in Figure 5, less than 1% of the droplet mass has been evaporated, while the mean temperature of the droplet increases by about 8K. This change of liquid temperature results in a decrease to its surface tension and viscosity equal to approximately 3% and 11%, respectively (properties based on [39] and [37], respectively).

The resulting non-dimensional numbers from the properties of Table 1 are: Oh=0.05, ε=51 and N=37. By changing the initial droplet velocity, the obtained We numbers range from 5 up to 60, while the Re number lies in the range of 240 to 832; it should be noted that for an isolated droplet these conditions correspond to the bag and multi-mode regimes. The examined non-dimensional distances measured from the droplet centers (H/D_0) range from 1.25 up to 20, resulting in 69 examined cases (two of which are in 3 dimensions with We=40 and H/D_0=2) in total (see Figure 1). Finally, 2-D axisymmetric simulations have been performed with an isolated droplet as well, using the same computational domain and conditions, resulting in 10 simulations in total in the range of We=15-60. These simulations are utilized in section 3.2 to calculate the quantities of the isolated droplet, which are compared with those of the droplet in a cluster; the quantities of both configurations are functions of the We number.

Table 1. Representative Diesel engine conditions.

	D_0 (μm)	P (bar)	T_g (K)	μ_g(kg/s·m)	ρ_g (kg/m^3)	T_L (K)	μ_L(kg/m·s)	ρ_L(kg/m^3)	σ (N/m)
Value	50	40	900	4E-05	15.48	335	0.0015	788.6	0.024
Reference	[40]	[41]	[41]	[42]	Ideal gas law	[41]	[37]	[37]	[39]

2.1 Comparison between the computational domains

Before proceeding to the discussion of the results, a comparison is made between the computational domains of Figure 2 in order to justify their selection for the corresponding simulations. Figure 3 presents the temporal evolution of droplets' shape (VOF iso-value of 0.5) as predicted by the simulation of a case with We=40 and H/D_0=2 using the 3D-4 and 3D-1 computational domains. As it is observed, the droplet shapes of the four droplets are identical between them as also with that of the single droplet (3D-1 domain). This is further justified by looking at Figure 4, which presents the temporal evolution of droplet deformation in both axes (cross-stream and streamwise) as well as the droplet velocity. The results of the 3D-4 and 3D-1 domains are identical for the droplet velocity, while a small deviation is observed for the droplet deformation after t/t_{sh}=1.1, which is attributed to the

micro-droplets that are detached from the parent droplet. In the following sections, only the results of the 3D-1 configuration are presented for simplicity. It should be noted that the cross-stream deformation in the 3D simulations varies in the Y-Z plane (see Figure 5). For reasons of simplicity, we have assumed that $D_{cr}=0.5*(D_y+D_z)$, without accounting for any disturbances in the diagonal direction of the Y-Z plane.

Turning now to the results of the 2D-axissymetric simulation, these are presented in Figure 4 as well. As it can be seen, they are close to those of the 3D simulations for the droplet deformation, while for the droplet velocity a small deviation is observed, up to approximately t/t_{sh}=1. Nevertheless, these differences are expected to decrease at higher droplet distances H/D_0, as the droplets in cluster formation tend to approach the behavior of an isolated droplet. The results of the 2-D axisymmetric simulations are utilized mainly for the parametric study of this work, since they require approximately 160 times less computational resources than the 3D-1 domain, in terms of CPU·hours.

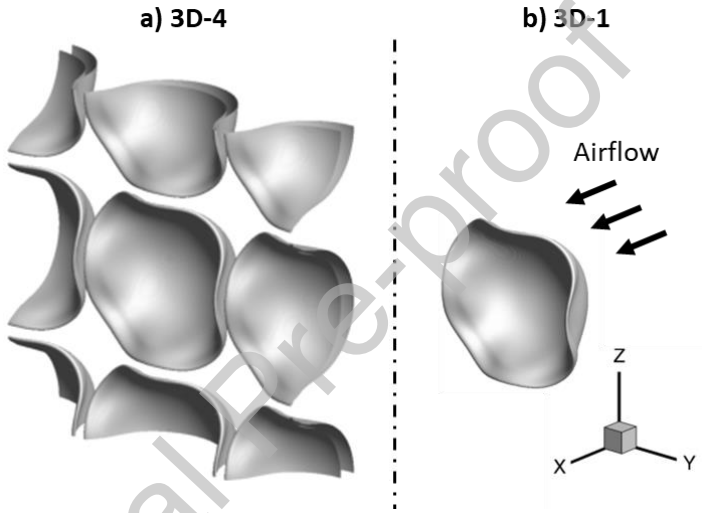

Figure 3. Droplet shape at the time instance of t/t_{sh}=1 as predicted by the simulation of a case with *We*=40 and H/D_0=2 using a) the 3D-4 and b) the 3D-1 computational domains.

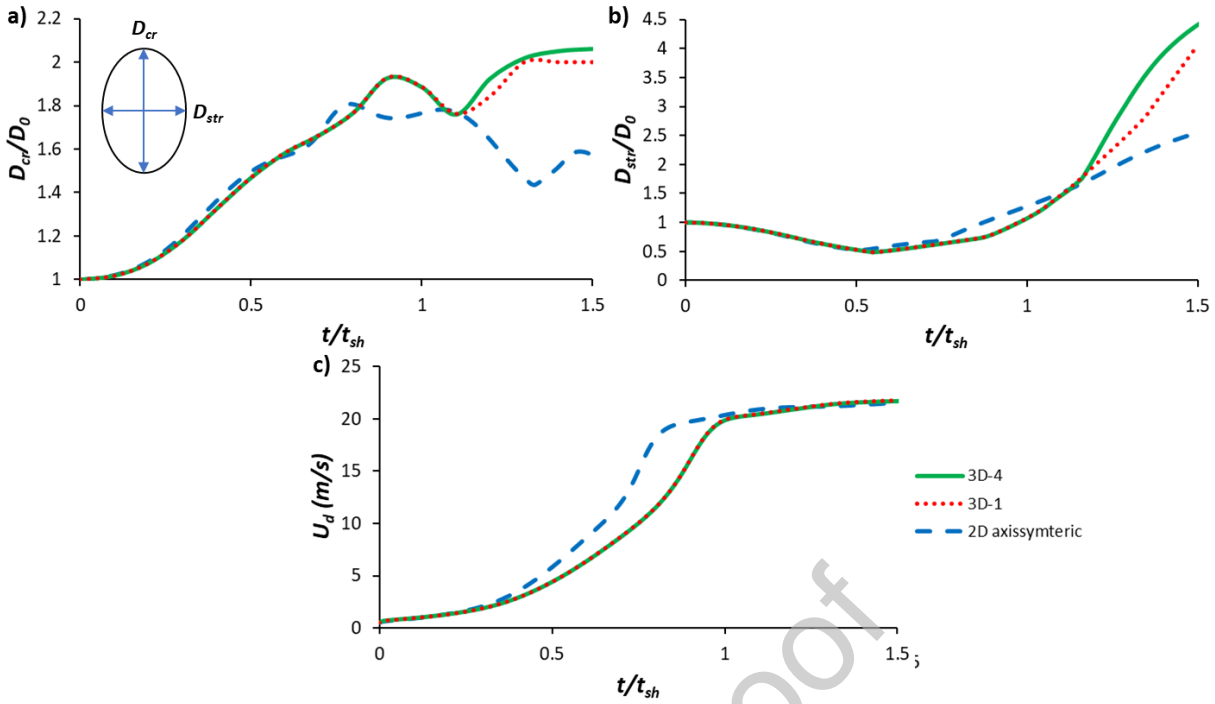

Figure 4. Temporal evolution of a) cross-stream droplet deformation, b) streamwise droplet deformation, and c) droplet velocity, as calculated by a simulation with We=40 and H/D_0=2 using the three computational domains: i) 3D-4, ii) 3D-1 and iii) the 2-D axisymmetric.

3 Results and discussion

3.1 Qualitative results

Figure 5 illustrates the temporal evolution of droplet shape as predicted both by the 3-D and the 2-D axisymmetric simulations (shape drawn with 3-D rotation around the x-axis) of a case with We=40 and H/D_0=2, as well as from the simulation of an isolated droplet at the same We number (2-D axisymmetric with 3-D rotation). As it is observed, the droplet in the cluster formation initially deforms into a disk-like shape (t/t_{sh}=0.4), followed by a semi-spherical shape (t/t_{sh}=0.8); breakup occurs with stripping of liquid from its periphery (t/t_{sh}=1.5). This breakup mode is called shuttlecock and has been identified in the authors' previous work for the breakup of droplets in tandem formation [4]; it is characterized by a large streamwise droplet deformation, while most of the liquid volume remains at its core. Turning now to the isolated droplet, it experiences the well-known multi-bag breakup regime, in which the droplet gradually deforms into a disk-like shape followed by the creation of a bag at its periphery (not shown here). In addition, its breakup occurs much slower compared to the cluster arrangement, at approximately t/t_{sh}=2.3 compared to t/t_{sh}=1.4 (and 1.2 in the 3-D simulation); this observation was also reported in the work of [6].

Regarding the comparison between the 2-D and 3-D simulations, they both predict similar droplet shapes up to t/t_{sh}=0.8, while after t/t_{sh}=1 a deviation is observed. At that time instance, the 3-D simulation predicts a wavy shape for the ring formed around the droplet, as shown in Figure 5 (t/t_{sh}=1). This is attributed, on the one hand, to the Kelvin-Helmholtz instabilities [43, 44], and on the other to bigger gap between the droplets in the diagonal direction compared to the vertical one. This causes non-uniform pressure and velocity distributions along the periphery of the droplet, as shown in Figure 6, where the Y-Z slices are presented for the dimensionless pressure ($(P-P_\infty)/\frac{1}{2}\rho_g U_{g,0}^2$)

and relative velocity (t/t_{sh}=0.9). Eventually, at t/t_{sh}=1.5 the waves turn into ligaments, since most of the liquid is concentrated at the corners of the droplet rather than its center.

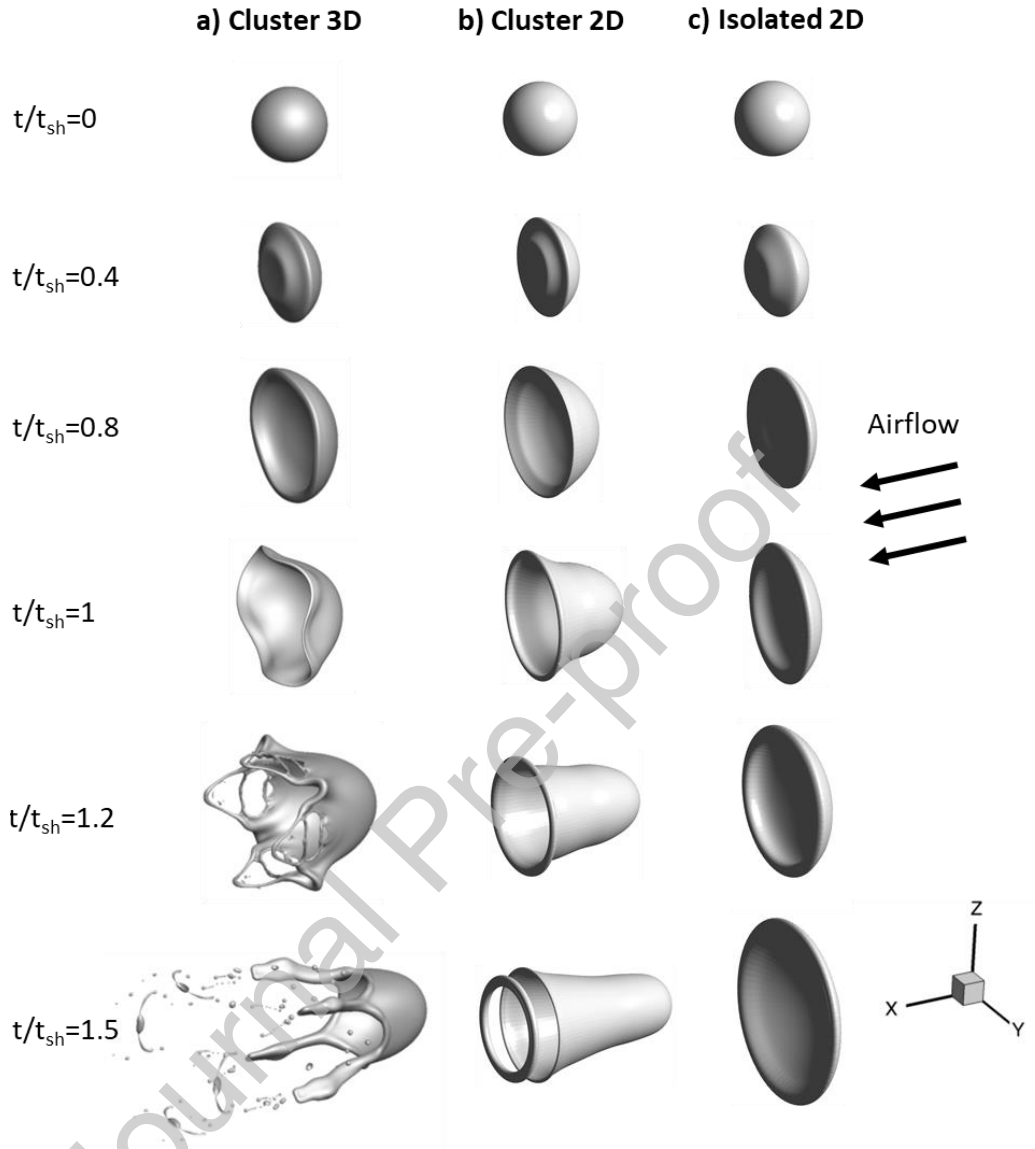

Figure 5. Temporal evolution of droplet shape as predicted by a) the 3-D simulation and b) the 2-D axisymmetric (3-D rotation) of a droplet in a cluster with H/D_0=2 and *We*=40, as well as an isolated droplet at the same *We* number.

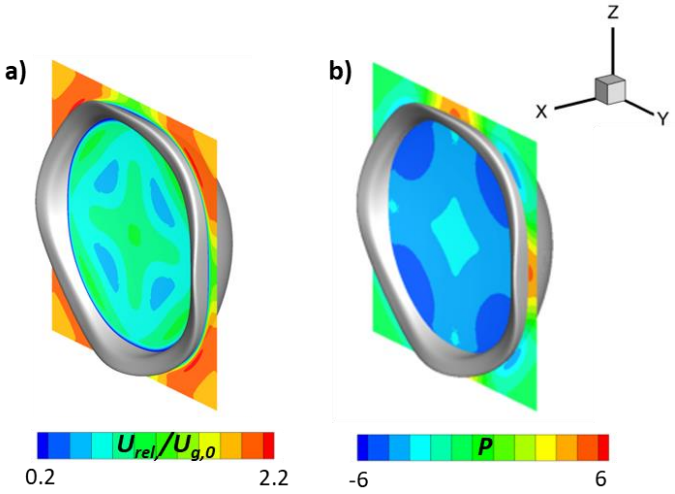

Figure 6. Y-Z slices of the dimensionless a) velocity and b) pressure as predicted by the 3-D simulation of a case with H/D_0=2 and We=40 (t/t_{sh}=0.9).

The differences in the shape and breakup modes of the isolated and cluster droplet arrangements are better explained by looking at Figure 7, which presents the contour of non-dimensional relative velocity for the same cases as those of Figure 5. In the cluster formation, the air accelerates in the narrow gap between the droplets (red color in the contour), causing the droplet to deform more at its periphery rather than its core. This results in the shifting of the breakup mode from multi-bag regime in the isolated droplet, to shuttlecock in the case of cluster arrangement.

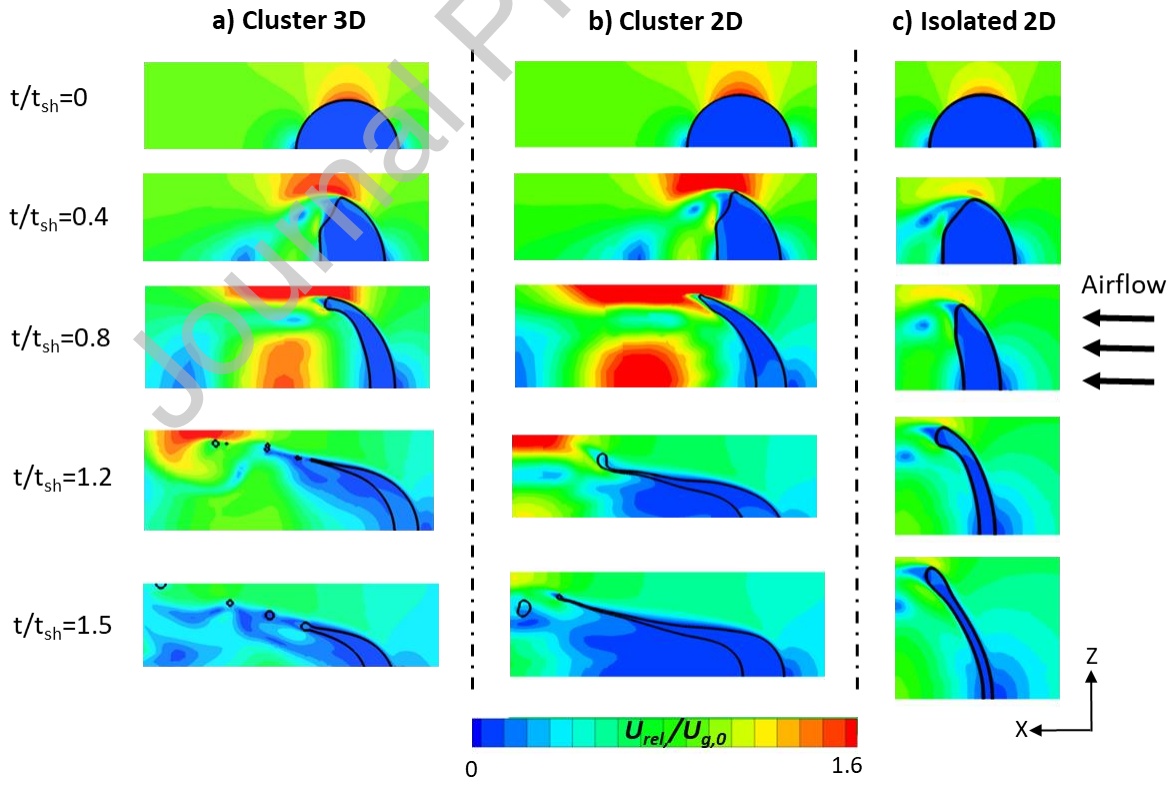

Figure 7. Non-dimensional relative velocity contour (X-Z plane) for a case of a droplet in a cluster (3-D and 2-D axisymmetric) with We=40 and H/D_0=2, as well as an isolated droplet at the same We number.

3.2 Parametric study

3.2.1 Breakup modes

In order to investigate the effect of distance between the droplets on the breakup mode, Figure 8 shows the temporal evolution of droplet shape for three cases corresponding to H/D_0=4, H/D_0=2 and H/D_0=1.25 (2-D axisymmetric domain). For large droplet distances and depending on the *We* number, the effect of the surrounding droplets is weak and the breakup mode becomes identical to that of the isolated droplet (bag breakup mode of Figure 8a). When the distance decreases, the breakup mode shifts from bag to deformation without breakup (Figure 8b), since the air flow is directed towards the periphery of the droplet, but without being intense enough to cause liquid stripping from its periphery. However, when the distance is further decreased, the air velocity becomes high enough to cause the breakup of the droplet, and the breakup mode shifts to shuttlecock (Figure 8c). This non-monotonic behaviour is better understood by looking at Figure 9, which presents a highlight of the dimensionless pressure contour $((P - P_\infty)/(\frac{1}{2}\rho_g U_{g,0}^2))$ for the three cases. For the larger droplet distances (H/D_0=4 in the figure), the pressure is higher at the core of droplet and lower at its periphery, causing the formation of the bag. At smaller distances (H/D_0=2), the peripheral pressure increases and becomes equal to the central, therefore preventing the creation of the bag. Finally, at even smaller distances (H/D_0=1.25), the peripheral pressure increases further causing the shuttlecock breakup mode.

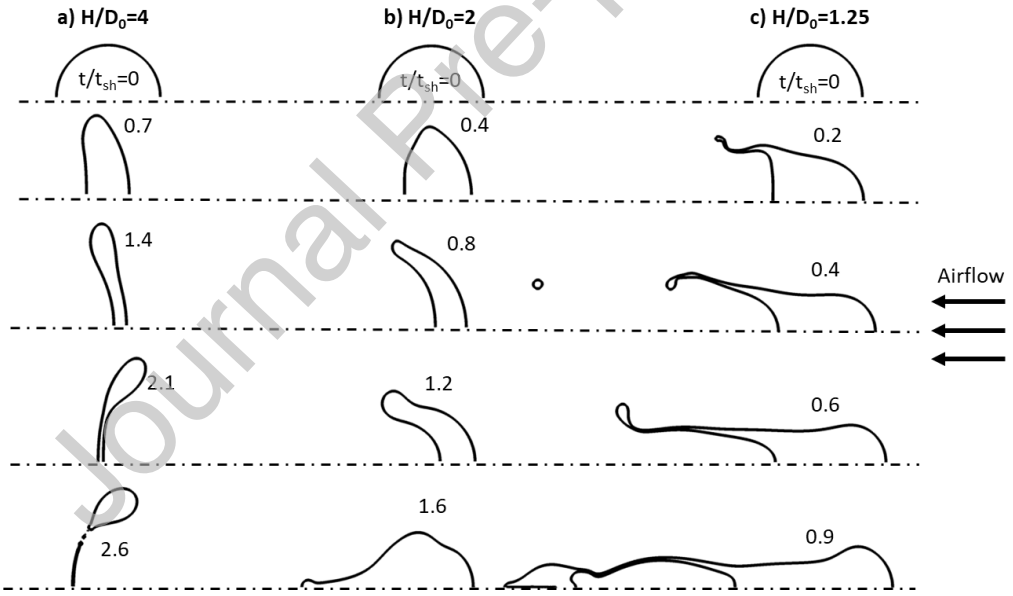

Figure 8. Temporal evolution of droplet shape for three cases with *We*=15 and: a) H/D_0=4, b) H/D_0=2 and c) H/D_0=1.25.

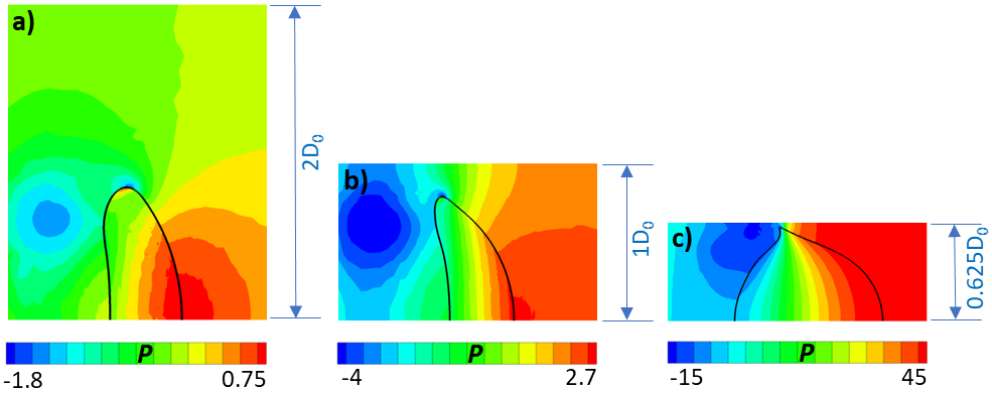

Figure 9. Dimensionless pressure contour for three cases with *We*=15 and: a) H/D_0=4 (t/t_{sh}=0.7), b) H/D_0=2 (t/t_{sh}=0.6) and c) H/D_0=1.25 (t/t_{sh}=0.1).

The aforementioned observations are summarized in Figure 10, which presents in a H/D_0-*We* map the simulated cases of the current work along with the encountered breakup regimes. For H/D_0≥4 the droplets behave as being isolated, i.e. the bag breakup regime is encountered for *We*≤20, while for *We*>20 they experience the multi-bag mode. For lower values of H/D_0 (<4) and low *We* numbers (≤30), the breakup mode shifts to deformation without breakup (Figure 8b). Finally, when the distance becomes even smaller (H/D_0≤2.5), the shuttlecock breakup regime is encountered, even for values of *We* number as low as 9, which is smaller than the value of the critical *We* number of an isolated droplet at the same conditions ($We_{cr,is}$=14).

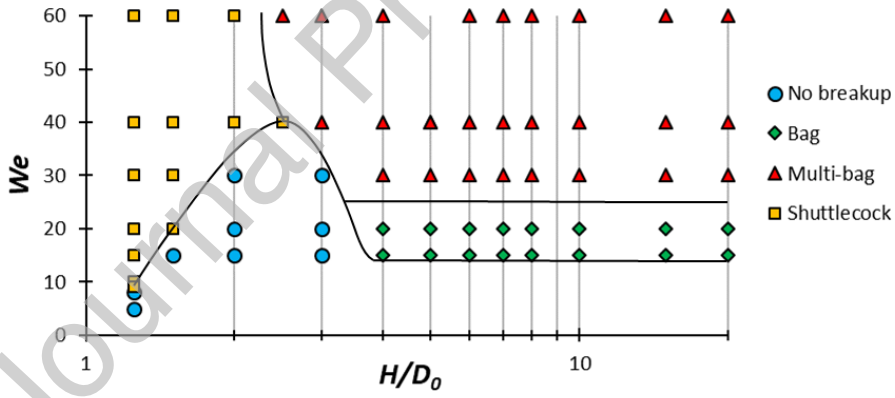

Figure 10. H/D_0-*We* map with the simulated cases of the current work along with the encountered breakup regimes (*Oh*=0.05, ε=51 and *N*=37).

3.2.2 Droplet surface area

The droplet surface area is an important quantity for spray applications and is calculated in the CFD simulations as $S = \sum_i^{n_{cells}} V_{cell}|\nabla a|$, which has been utilized also in [36, 38, 45, 46] and is derived using the divergence theorem (or Gauss theorem) for the volume fraction at the interface cells. The ratio of the maximum surface area of a droplet in a parallel moving cluster, to the maximum surface area of an isolated droplet ($S_{max,cl}/S_{max,is}$) is presented in Figure 11. The ratio $S_{max,cl}/S_{max,is}$ takes very low values at high *We* and low H/D_0, reaching values as low as 0.22, which corresponds to a 78% reduction in the maximum surface area of a droplet in cluster formation, relative to the one of an isolated droplet at the same *We*. This is attributed to the very fast breakup occurring at these

conditions, with liquid stripped from its periphery, while its core remains relatively non-deformed. On the other hand, at low *We* and H/D_0 the ratio $S_{max,cl}/S_{max,is}$ is greater than 1, reaching values as high as 1.29, owing to the very large streamwise droplet deformation (Figure 8c). Finally, the solid line of Figure 11 defines the region of influence of the maximum surface area of a droplet in cluster formation; this occurs for droplet distances of approximately $H/D_0 \leq 5$.

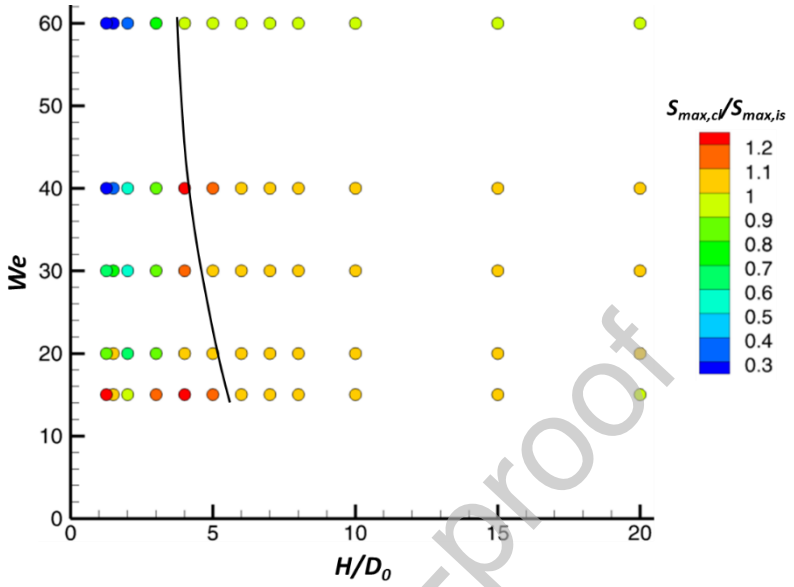

Figure 11. Ratio $S_{max,cl}/S_{max,is}$ as function of *We* and H/D_0. The black line defines the region of influence of the maximum surface area of a droplet in cluster formation.

3.2.3 Breakup initiation time

As already mentioned in Section 3.1, a droplet inside a parallel moving cluster breaks up faster than an isolated droplet. The breakup initiation time (t_{br}), which is defined as the time instance that a micro-droplet detaches from the parent droplet for the first time, is measured manually in the simulations using a visual representation of the process. The ratio $t_{br,cl}/t_{br,is}$ is presented in Figure 12 as function of the *We* number and the H/D_0. The ratio $t_{br,cl}/t_{br,is}$ decreases with decreasing H/D_0, reaching values as low as 0.1. As can be seen from the figure, the breakup time of the cluster formation is different from that of the isolated at distances $H/D_0 \leq 3$.

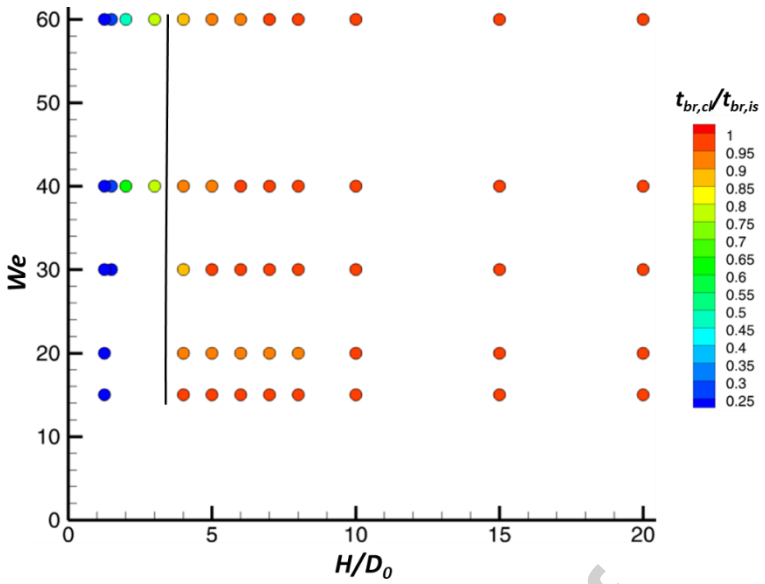

Figure 12. Ratio $t_{br,cl}/t_{br,is}$ as function of *We* and H/D_0. The black line defines the region of influence of the breakup time of a droplet in cluster formation.

3.2.4 Drag coefficient

The drag coefficient (C_d) is calculated using the droplet momentum balance on the droplet with the effect of virtual mass and Basset forces incorporated into the C_d, similar to previous numerical studies [47-50]. The effect of droplet frontal area can either i) be incorporated into the drag coefficient and ii) assumed to vary linearly with time $\frac{A_f(t^*)}{A_{f,0}} = 1 + B \cdot t^*$. The following equations, (3) and (4), are derived based on the two approaches, respectively, and give the temporal evolution of droplet velocity (their derivation can be found in our previous work [38]). The average drag coefficient is found for each simulated case by fitting the equations to the results of the simulations ($U_d - t^*$), as shown in Figure 14 and Figure 13, where the ratios $C_{d,cl}/C_{d,is}$ are presented as function of the *We* number and the H/D_0, using the two approaches. The ratio $C_{d,cl}/C_{d,is}$ increases with decreasing H/D_0, reaching values as high as 29 for the first approach and 15 for the second one. This trend is in agreement with the works of [1, 15, 17-19]. Overall, the drag coefficient of droplets in cluster formations differs from that of the isolated droplet for distances $H/D_0 \leq 3$ for the first method, and $H/D_0 \leq 2$ for the second.

$$U_d(t^*) = \frac{U_{g,0}}{\overline{C_d}\left(\frac{3}{4}\right)\left(\frac{1}{\sqrt{\varepsilon}}\right)t^* + 1} \tag{3}$$

$$U_d(t^*) = \frac{U_{g,0}}{\overline{C_d}\left(\frac{3}{4}\right)\left(\frac{1}{\sqrt{\varepsilon}}\right)(t^* + \frac{B \cdot (t^*)^2}{2}) + 1} \tag{4}$$

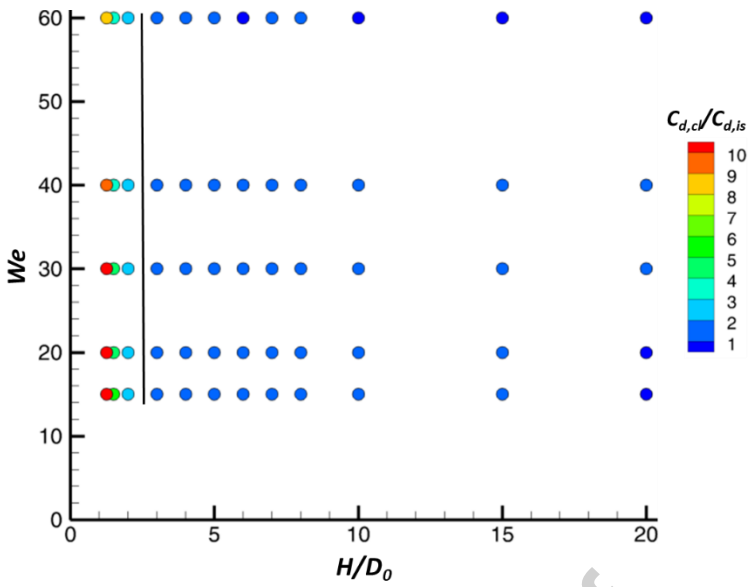

Figure 13. Ratio $C_{d,cl}/C_{d,is}$ as function of *We* and H/D_0. The effect of droplet frontal area is incorporated in the drag coefficient. The black line defines the region of influence of the drag coefficient of a droplet in cluster formation.

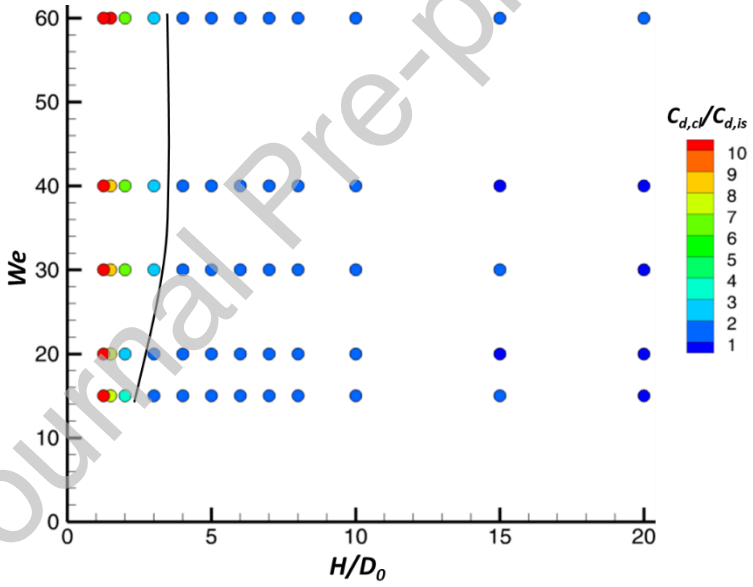

Figure 14. Ratio $C_{d,cl}/C_{d,is}$ as function of *We* and H/D_0. The droplet frontal area varies linearly with time. The black line defines the region of influence of the drag coefficient of a droplet in cluster formation.

4 Conclusions

In the current work, 2-D axisymmetric and 3-D simulations were performed with Diesel droplets in a parallel moving cluster. The examined *We* numbers range from 5 up to 60 and non-dimensional distances between them (H/D_0) from 1.25 up to 20. It was found that for droplet distances $H/D_0 \leq 2.5$ and depending on the *We* number, the droplets experience the so-called shuttlecock breakup mode, which is characterized by a stretching of the droplet at its periphery, similar to the droplets in tandem formations [4]. This is caused by the high air velocities developed at the gap between the

droplets. Furthermore, their breakup occurs faster and experience higher drag coefficients compared to the isolated droplets, effects which are amplified as the distance between the droplets (H/D_0) decreases. At very low droplet distances H/D_0<1.5, the critical *We* number of a droplet in a cluster becomes lower than that of an isolated droplet at the same conditions. Overall, it is found that the droplets are affected by the presence of other droplets in the cross-stream direction for distances $H/D_0 \leq 5$.

Acknowledgements

Financial support from the MSCA-ITN-ETN of the European Union's H2020 programme, under REA grant agreement n. 675676 is acknowledged.

References

[1] Ashgriz, N., 2011, Handbook of atomization and sprays: theory and applications, Springer Science & Business Media.
[2] Guildenbecher, D. R., López-Rivera, C., and Sojka, P. E., 2009, "Secondary atomization," Experiments in Fluids, 46(3), pp. 371-402.
[3] Nicholls, J. A., and Ranger, A. A., 1969, "Aerodynamic shattering of liquid drops," AIAA Journal, 7(2), pp. 285-290.
[4] Stefanitsis, D., Malgarinos, I., Strotos, G., Nikolopoulos, N., Kakaras, E., and Gavaises, M., 2018, "Numerical investigation of the aerodynamic breakup of droplets in tandem," International Journal of Multiphase Flow.
[5] Temkin, S., and Ecker, G. Z., 1989, "Droplet pair interactions in a shock-wave flow field," Journal of Fluid Mechanics, 202, pp. 467-497.
[6] Kékesi, T., Altimira, M., Amberg, G., and Wittberg, L. P., 2019, "Interaction between two deforming liquid drops in tandem and various off-axis arrangements subject to uniform flow," International Journal of Multiphase Flow, 112, pp. 193-218.
[7] Ozgoren, M., Dogan, S., Canli, E., Akilli, H., and Sahin, B., 2014, "Comparison of Different Configurations of Two Spheres at Re= 5000 in a Uniform Flow," 17th International Symposiumon Applications o fLaser Techniques to Fluid Mechanics Lisbon, Portugal.
[8] Pinar, E., Sahin, B., Ozgoren, M., and Akilli, H., 2013, "Experimental study of flow structures around side-by-side spheres," Industrial & Engineering Chemistry Research, 52(40), pp. 14492-14503.
[9] Folkersma, R., Stein, H., and Van de Vosse, F., 2000, "Hydrodynamic interactions between two identical spheres held fixed side by side against a uniform stream directed perpendicular to the line connecting the spheres' centres," International Journal of Multiphase Flow, 26(5), pp. 877-887.
[10] Tsuji, T., Narutomi, R., Yokomine, T., Ebara, S., and Shimizu, A., 2003, "Unsteady three-dimensional simulation of interactions between flow and two particles," International Journal of Multiphase Flow, 29(9), pp. 1431-1450.
[11] Ardekani, A., and Rangel, R., 2006, "Unsteady motion of two solid spheres in Stokes flow," Physics of Fluids, 18(10), p. 103306.
[12] Prahl, L., Hölzer, A., Arlov, D., Revstedt, J., Sommerfeld, M., and Fuchs, L., 2007, "On the interaction between two fixed spherical particles," International Journal of Multiphase Flow, 33(7), pp. 707-725.
[13] Yoon, D.-H., and Yang, K.-S., 2007, "Flow-induced forces on two nearby spheres," Physics of Fluids, 19(9), p. 098103.
[14] Jadoon, A., Prahl, L., and Revstedt, J., 2010, "Dynamic interaction of fixed dual spheres for several configurations and inflow conditions," European Journal of Mechanics-B/Fluids, 29(1), pp. 43-52.
[15] Connon, C., and Dunn-Rankin, D., 1996, "Flow behavior near an infinite droplet stream," Experiments in Fluids, 21(2), pp. 80-86.
[16] Zhao, H., Wu, Z., Li, W., Xu, J., and Liu, H., 2019, "Interaction of two drops in the bag breakup regime by a continuous air jet," Fuel, 236, pp. 843-850.
[17] Kim, I., Elghobashi, S., and Sirignano, W., 1991, "Three-dimensional droplet interactions in dense sprays," 29th Aerospace Sciences Meeting, American Institute of Aeronautics and Astronautics.
[18] Kim, I., Elghobashi, S., and Sirignano, W., "Three-dimensional flow computation for two interacting, moving droplets," Proc. AIAA Materials Specialist Conference-Coating Technology for Aerospace Systems.
[19] Prahl, L., Revstedt, J., and Fuchs, L., "Interaction among droplets in a uniform flow at intermediate Reynolds numbers," Proc. 44th AIAA Aerospace Sciences Meeting and Exhibit, Reno, Nevada, USA, January, pp. 9-12.
[20] Hirt, C. W., and Nichols, B. D., 1981, "Volume of fluid (VOF) method for the dynamics of free boundaries," Journal of Computational Physics, 39(1), pp. 201-225.
[21] Lafaurie, B., Nardone, C., Scardovelli, R., Zaleski, S., and Zanetti, G., 1994, "Modelling Merging and Fragmentation in Multiphase Flows with SURFER," Journal of Computational Physics, 113(1), pp. 134-147.
[22] "ANSYS®FLUENT, 2014, Release 16.0."

[23] Malgarinos, I., Nikolopoulos, N., and Gavaises, M., 2015, "Coupling a local adaptive grid refinement technique with an interface sharpening scheme for the simulation of two-phase flow and free-surface flows using VOF methodology," Journal of Computational Physics, 300, pp. 732-753.
[24] Strotos, G., Malgarinos, I., Nikolopoulos, N., and Gavaises, M., 2016, "Numerical investigation of aerodynamic droplet breakup in a high temperature gas environment," Fuel, 181, pp. 450-462.
[25] Malgarinos, I., Nikolopoulos, N., Marengo, M., Antonini, C., and Gavaises, M., 2014, "VOF simulations of the contact angle dynamics during the drop spreading: Standard models and a new wetting force model," Advances in Colloid and Interface Science, 212, pp. 1-20.
[26] Malgarinos, I., Nikolopoulos, N., and Gavaises, M., 2016, "A numerical study on droplet-particle collision dynamics," International Journal of Heat and Fluid Flow, 61, Part B, pp. 499-509.
[27] Malgarinos, I., Nikolopoulos, N., and Gavaises, M., 2017, "Numerical investigation of heavy fuel droplet-particle collisions in the injection zone of a Fluid Catalytic Cracking reactor, Part I: Numerical model and 2D simulations," Fuel Processing Technology, 156, pp. 317-330.
[28] Malgarinos, I., Nikolopoulos, N., and Gavaises, M., 2017, "Numerical investigation of heavy fuel droplet-particle collisions in the injection zone of a Fluid Catalytic Cracking reactor, part II: 3D simulations," Fuel Processing Technology, 156, pp. 43-53.
[29] G. Strotos, I. M., N. Nikolopoulos, K. Papadopoulos, A. Theodorakakos, M.Gavaises, 2015, "Performance of VOF methodology in predicting the deformation and breakup of impulsively accelerated droplets," ICLASS 2015, 13th Triennial International Conference on Liquid Atomization and Spray Systems, August 23-27Tainan, Taiwan.
[30] Strotos, G., Malgarinos, I., Nikolopoulos, N., and Gavaises, M., 2016, "Predicting droplet deformation and breakup for moderate Weber numbers," International Journal of Multiphase Flow, 85, pp. 96-109.
[31] Strotos, G., Malgarinos, I., Nikolopoulos, N., and Gavaises, M., 2016, "Aerodynamic breakup of an n-decane droplet in a high temperature gas environment," Fuel, 185, pp. 370-380.
[32] Stefanitsis, D., Malgarinos, I., Strotos, G., Nikolopoulos, N., Kakaras, E., and Gavaises, M., 2017, "Numerical investigation of the aerodynamic breakup of Diesel and heavy fuel oil droplets," International Journal of Heat and Fluid Flow, 68, pp. 203-215.
[33] Stefanitsis, D., Malgarinos, I., Strotos, G., Nikolopoulos, N., Kakaras, E., and Gavaises, M., 2017, "Numerical investigation of the aerodynamic breakup of Diesel droplets under various gas pressures," 28th Conference on Liquid Atomization and Spray Systems (ILASS-Europe 2017)Valencia, Spain.
[34] Stefanitsis, D., Strotos, G., Nikolopoulos, N., Kakaras, E., and Gavaises, M., 2018, "Numerical examination of the aerodynamic breakup of droplets in chain formation," 14th Triennial International Conference on Liquid Atomization and Spray Systems (ICLASS 2018)Chicago, USA.
[35] Stefanitsis, D., Strotos, G., Nikolopoulos, N., Kakaras, E., and Gavaises, M., 2019, "Improved droplet breakup models for spray applications," International Journal of Heat and Fluid Flow, 76, pp. 274-286.
[36] Strotos, G., Malgarinos, I., Nikolopoulos, N., and Gavaises, M., 2016, "Predicting the evaporation rate of stationary droplets with the VOF methodology for a wide range of ambient temperature conditions," International Journal of Thermal Sciences, 109, pp. 253-262.
[37] Vidal, A., Rodriguez, C., Koukouvinis, P., Gavaises, M., and McHugh, M. A., "Modelling of Diesel fuel properties through its surrogates using Perturbed-Chain, Statistical Associating Fluid Theory," International Journal of Engine Research, 0(0), p. 1468087418801712.
[38] Stefanitsis, D., Malgarinos, I., Strotos, G., Nikolopoulos, N., Kakaras, E., and Gavaises, M., 2019, "Numerical investigation of the aerodynamic breakup of droplets in tandem," International Journal of Multiphase Flow, 113, pp. 289-303.
[39] Yaws, C. L., and Gabbula, C., 2003, Yaws" Handbook of Thermodynamic and Physical Properties of Chemical Compounds, Knovel.
[40] Wadhwa, A. R., Magi, V., and Abraham, J., 2007, "Transient deformation and drag of decelerating drops in axisymmetric flows," Physics of Fluids (1994-present), 19(11), p. 113301.
[41] Lacaze, G., Misdariis, A., Ruiz, A., and Oefelein, J. C., 2015, "Analysis of high-pressure Diesel fuel injection processes using LES with real-fluid thermodynamics and transport," Proceedings of the Combustion Institute, 35(2), pp. 1603-1611.
[42] Sutherland, W., 1893, "LII. The viscosity of gases and molecular force," The London, Edinburgh, and Dublin Philosophical Magazine and Journal of Science, 36(223), pp. 507-531.
[43] Theofanous, T. G., 2011, "Aerobreakup of Newtonian and Viscoelastic Liquids," Annual Review of Fluid Mechanics, 43(1), pp. 661-690.
[44] Lee, C. H., and Reitz, R. D., 2000, "An experimental study of the effect of gas density on the distortion and breakup mechanism of drops in high speed gas stream," International Journal of Multiphase Flow, 26(2), pp. 229-244.
[45] Strotos, G., Gavaises, M., Theodorakakos, A., and Bergeles, G., 2008, "Numerical investigation on the evaporation of droplets depositing on heated surfaces at low Weber numbers," International Journal of Heat and Mass Transfer, 51(7-8), pp. 1516-1529.
[46] Strotos, G., Gavaises, M., Theodorakakos, A., and Bergeles, G., 2011, "Numerical investigation of the evaporation of two-component droplets," Fuel, 90(4), pp. 1492-1507.
[47] Quan, S., and Schmidt, D. P., 2006, "Direct numerical study of a liquid droplet impulsively accelerated by gaseous flow," Physics of Fluids (1994-present), 18(10), p. 102103.
[48] Khare P., V. Y., "Drag Coefficients of Deforming and Fragmenting Liquid Droplets," Proc. ILASS Americas, 25th Annual Conference on Liquid Atomization and Spray Systems.

[49] Yang, W., Jia, M., Sun, K., and Wang, T., 2016, "Influence of density ratio on the secondary atomization of liquid droplets under highly unstable conditions," Fuel, 174, pp. 25-35.
[50] Shao, C., Luo, K., and Fan, J., 2017, "Detailed numerical simulation of unsteady drag coefficient of deformable droplet," Chemical Engineering Journal, 308, pp. 619-631.